Arroyo, M. *et al.* (2011). *Géotechnique* **61**, No. 6, 525–531 [**doi:** 10.1680/geot.9.P.067]

TECHNICAL NOTE

Cone penetration tests in a virtual calibration chamber

M. ARROYO*, J. BUTLANSKA*, A. GENS*, F. CALVETTI† and M. JAMIOLKOWSKI‡

A virtual calibration chamber was built using a three-dimensional model based on the discrete-element method. The chamber was then filled with a scaled granular equivalent of Ticino sand, the material properties of which were selected by curve-fitting triaxial tests. Cone penetration tests were then performed under different initial densities and isotropic stresses. Penetration resistance in the virtual calibration chamber was affected by the same cone/chamber size effect that affects physical calibration chambers and was corrected accordingly. The corrected cone resistance obtained from the virtual calibration chamber cone penetration tests shows good quantitative agreement with correlations that summarise previous physical results.

KEYWORDS: in situ testing; laboratory testing; numerical modelling; sands

On réalise une chambre de calibrage virtuelle [*virtual calibration chamber* (VCC)] en utilisant un modèle tridimensionnel basé sur une méthode aux éléments discrets. On remplit ensuite la chambre avec une matière granulaire étalonnée équivalente au sable du Tessin, dont les propriétés matérielles ont été sélectionnées par des tests triaxiaux à ajustement analytique. On effectue ensuite des essais de pénétrabilité au cône sous différentes densités initiales et contraintes isotropes. La résistance à la pénétration dans le VCC a été affectée par le même effet de taille cône/chambre qui affecte les chambres de calibrage physiques, et rectifiée en conséquence. La résistance corrigée au cône, obtenue avec les essais de pénétrabilité au cône sur la chambre de calibrage virtuelle, indique une bonne correspondance quantitative avec des corrélations qui résument des résultats physiques précédents.

INTRODUCTION

The cone penetration test (CPT) is a major tool in geotechnical site characterisation. Interpretation of CPT results in clay has advanced considerably from a theoretical viewpoint (e.g. Randolph, 2004) but in sands it still largely relies on empirical correlations (Mayne, 2007). A major source of such correlations is work performed in calibration chambers (CCs), where soil state and properties are tightly controlled (Huang & Hsu, 2004). Calibration chamber testing is usually expensive and time-consuming, hence complementing the physical tests with virtual equivalents is an attractive idea. If virtual tests could be run on numerical models of the calibration chamber, this would allow the extension, extrapolation and, in some cases, substitution of physical test series.

To achieve meaningful virtual tests it is necessary

(*a*) to prove that the virtual calibration chamber (VCC) is able to reproduce quantitatively the results obtained in equivalent physical tests
(*b*) to provide a clear methodology to build the VCC.

The purpose of this note is to show that these requirements are attainable with three-dimensional models based on the discrete-element method (DEM).

Numerical models of CPT in sands

Huang & Ma (1994), Calvetti & Nova (2005) and Jiang *et al.* (2006) have all presented DEM-based two-dimensional models of cone penetration tests. Qualitative insight was gained, but the intrinsic limitations of disc-based models precluded quantitative comparisons with physical tests.

Susila & Hryciw (2003) employed finite elements to simulate CPTs in sands. Some quantitative agreement with experimental CC tests was obtained. Ahmadi *et al.* (2005) used finite differences and presented a systematic comparison with the same reference database described below. The mean error on predicted CPT resistance ranged from 15 to 30%, depending on the selected boundary condition. A somewhat complex calibration procedure was required in both cases.

Reference database

The physical calibration chamber CPT reference test series was performed on Ticino sand at Instituto Sperimentale Modelli e Strutture (ISMES) in Bergamo and Ente Nazionale per l'Energía Elettrica (ENEL) in Milan (Jamiolkowski *et al.*, 2003). Ticino sand is a poorly graded medium-sized sand, with mostly sub-rounded grains. Some of its properties are listed in Table 1. The grain size distribution is illustrated in Fig. 1.

Calibration chamber testing is affected by chamber size effects (Parkin & Lunne, 1982). For stress-controlled boundary conditions (BC1 type), an empirical correction factor, CF, is applied to extrapolate to field conditions (Jamiolkowski *et al.*, 2003)

$$\mathrm{CF} = a(D_\mathrm{R})^b \tag{1}$$

Butlanska *et al.* (2010) show that

$$a = 9 \times 10^{-5} R_\mathrm{d}^{2\cdot02}$$
$$b = -0\cdot565 \ln(R_\mathrm{d}) + 2\cdot59 \tag{2}$$

where $R_\mathrm{d} = D_\mathrm{C}/d_\mathrm{c}$, is the ratio of chamber diameter, D_C, to cone diameter, d_c.

The CC CPT database results were summarised by several empirical relationships between corrected cone resistance,

Manuscript received 21 May 2009; revised manuscript accepted 17 June 2010. Published online ahead of print 25 November 2010. Discussion on this paper closes on 1 November 2011, for further details see p. ii.
* Departamento de Ingeniería del Terreno, UPC, Barcelona, Spain.
† Dipartimento di Ingegnieria Strutturale, Politecnico di Milano, Italy.
‡ Dipartimento di Ingegneria Strutturale e Geotecnica, Politecnico di Torino, Italy.

Table 1. Ticino sand properties and grain size characteristics of the DE models (ET – element test; CC – calibration chamber)

	D_{50}: mm	C_u: mm	D_{min}: mm	e_{min}	e_{max}
Ticino sand	0·53	1·61	0·09	0·578	0·924
DEM ET	0·54	1·70	0·3	—	—
DEM CC	26·6	1·68	4·5	—	—

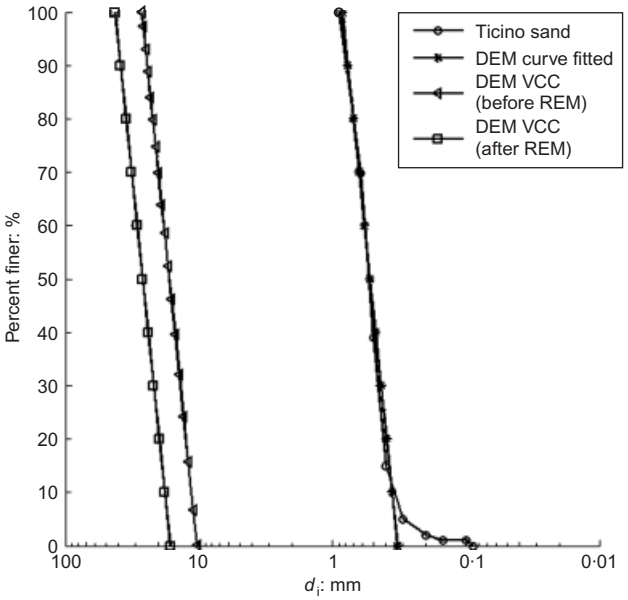

Fig. 1. Grain size distribution (gsd) of Ticino sand and DEM models

q_c^*, relative density and a stress measure. For normally consolidated and overconsolidated Ticino sand, a highly significant correlation was found (Jamiolkowski *et al.*, 2003) using relative density, D_R, and effective mean stress, p'

$$q_c^* = 23{\cdot}19\, p_a \left(\frac{p'}{p_a}\right)^{0{\cdot}56} e^{2{\cdot}97 D_R} \tag{3}$$

where p_a is the atmospheric pressure.

MODELLING APPROACH

Numerical method

The DEM code PFC3D (Itasca, 2005) was employed. The discrete elements were always spherical in shape. Particle rotation was prevented, to mimic roughly the effect of non-spherical particle shapes. It is known (Ting *et al.*, 1989) that this is key to achieve realistic macroscopic friction angles with spherical particles.

The contact law employed is elasto-plastic. The elastic part is linear and the normal and tangential stiffness at any contact, k_N and k_S, are described by the following scaling rule

$$k_N = 2K_{eff}\frac{D_1 D_2}{D_1 + D_2} \qquad k_S = \alpha\, k_N \tag{4}$$

This choice has proven useful in other geotechnical problems (Calvetti, 2008). Model parsimony explains the fixed ratio between normal and shear stiffness; this parameter affects the results only marginally.

The plastic part of the contact law was frictional, defined by the interparticle friction angle, Φ_μ. No cohesion was included in the contact model. The simulations employed numerical non-viscous damping (Cundall, 1987). This is equivalent to suppress mechanical wave propagation in the system and it is particularly useful to achieve rapid convergence in quasi-static problems.

Calibration procedure

Within the framework outlined, there are four material constants to calibrate: those related to stiffness, (K_{eff}, α), interparticle friction, Φ_μ, and damping. The values for these constants were selected using DEM models to simulate element tests in Ticino sand. A cubical DEM cell representing a Ticino sand specimen was constructed. It had an 8 mm length side and contained 4700 particles within rigid walls. The grain size distribution of the model reproduced Ticino sand, with a truncation to exclude fines (Fig. 1). Specimens were built to specified porosity using the radius expansion method (REM) (Itasca, 2005).

Calibration was performed using results from an isotropically compressed drained triaxial test (TEST M09) confined at 100 kPa and formed with $D_R = 75\%$. By trial and error a satisfactory match was obtained (Fig. 2) using the following set of parameters: $K_{eff} = 300$ MPa, $\alpha = 0{\cdot}25$ and $\mu = 0{\cdot}35$ (equivalent to an interparticle friction angle, Φ_μ, of 19·3). Damping was set at 0·05. The parameter set obtained in this way led to a successful reproduction of other drained triaxial tests, at different confining stresses (110, 200 and 300 kPa) and initial relative densities (45%, 75% and 90%) (Butlanska, 2009).

Model constraints and grain-size scaling

It is possible to write an estimate of the number of particles in the model, N, as follows

$$N = f_G \frac{3}{2}\, n_p^3\, R_d^2\, n_h (1 - n) \tag{5}$$

where n represents porosity and the three adimensional ratios are

$$n_p = \frac{d_c}{D_{50}} \qquad R_d = \frac{D_C}{d_c} \qquad n_h = \frac{H}{d_c} \tag{6}$$

where H is the CC height and D_{50} is the characteristic grain diameter. f_G is an empirical factor accounting for the grain size distribution shape (roughly 1·3 for the fine-truncated Ticino sand). As Table 2 illustrates, a model that maintained the original CC dimensions and mean grain size of Ticino sand would require more than 1E10 particles. That number is beyond current computational abilities.

To achieve a manageable number of particles, a uniform scaling factor of 50 was applied to the grain size distribution, the cone size was multiplied by 2 from that in the physical tests and the calibration chamber was shortened by another factor of 2. As can be seen in Table 2, this resulted in 65 000 elements in the densest specimens, almost an order of magnitude more than the number employed in previous two-dimensional studies.

Model construction

The cone shaft (Fig. 3) is described with four rigid cylindrical walls: one frictionless and three frictional. The tip had an angle of 60° and is also frictional. Perfect roughness was assumed in the contact between cone and particles, with friction equal to the interparticle one ($\mu = 0{\cdot}35$). The calibration chamber walls are frictionless.

Both the cone and the CC have cylindrical symmetry. In

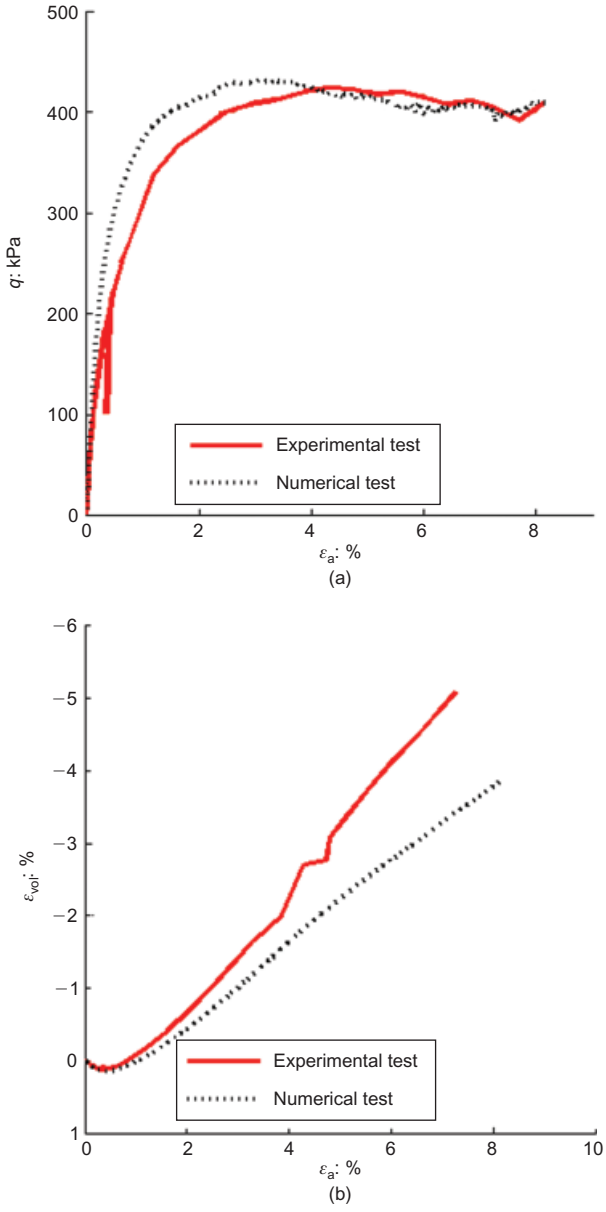

Fig. 2. Calibration of DEM material parameters with a triaxial test on Ticino sand ($D_R = 75\%$, $p_0 = 100$ kPa). Experimental results and simulations with cubical DE cells

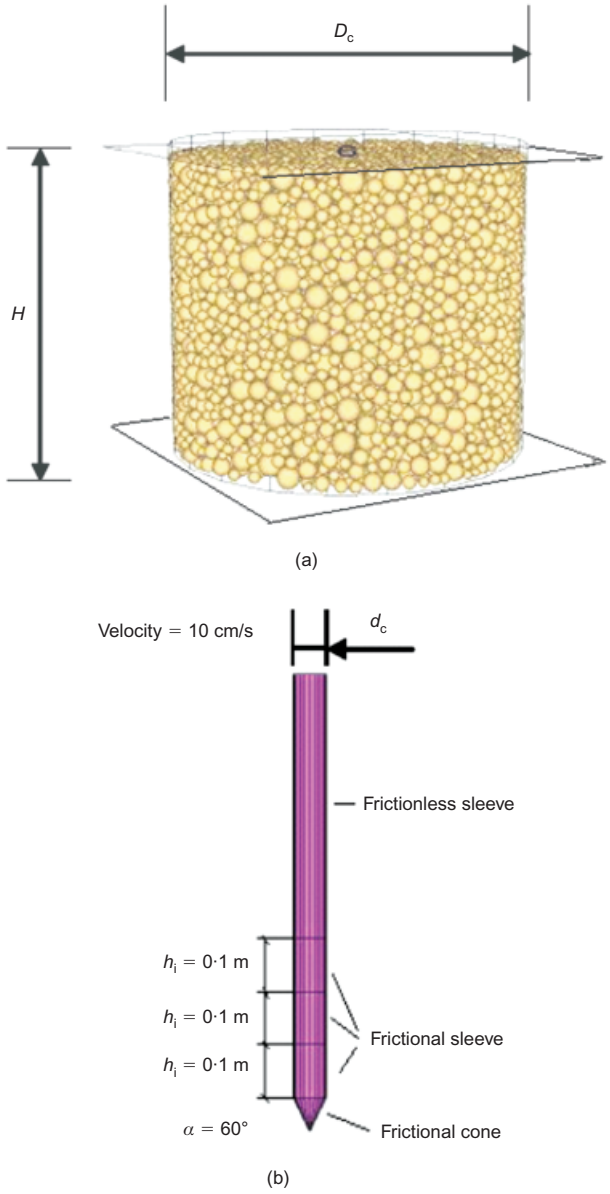

Fig. 3. View of the DEM model components with indication of the main relevant dimensions: (a) calibration chamber; (b) cone

Table 2. Summary of geometrical characteristics and estimate of model particle requirements in various cases

Case	ISMES CC Ticino sand	3D DEM model (present study)	Ma (1994)†	Calvetti & Nova (2005)†	Jiang *et al.* (2006)†
d_c: mm	35·6	71·2	10	100	36
D_c: mm	1200	1200	160	1200	630
D_{50}: mm	0·53	26·5	0·8	13·5	2·925
H: mm	1500	700	97·5	1500	288
n_p	67	2·7	12·5	7·4	12·3
R_d	33·7	16·9	16	12	17·5
n_h	16·9	9·8	9·8	15	8
N_{3D}*	$1{\cdot}8 \times 10^{10}$	$6{\cdot}5 \times 10^4$	$5{\cdot}9 \times 10^6$	$1{\cdot}1 \times 10^6$	$5{\cdot}5 \times 10^6$
N_{eff}	—	$6{\cdot}5 \times 10^4$	$<1{\cdot}8 \times 10^4$	$1{\cdot}0 \times 10^4$	$1{\cdot}0 \times 10^4$

* Porosity $n = 0{\cdot}38$ and grain size distribution factor $f_g = 1{\cdot}3$ are assumed.
† The authors employed two-dimensional models.

principle, frictionless radial walls stopping the circumferential motion of particles can be used to enforce that symmetry and reduce computational expense. Butlanska *et al.* (2009) show that, despite some micro-heterogeneity, changes in the macro response of the model using full, half and quarter chambers are small.

Specimens were created to a relative density slightly above the target value using the REM. Velocities were then reset to zero. Isotropic compression to 10 kPa in which the interparticle friction might be reduced was used to obtain – by trial and error – a closer fit (within 5%) to the relative density target. Interparticle friction was then reset to the calibrated value and isotropic stress ramped up to the target value. After equilibration, cone penetration proceeded at 10 cm/s. A constant stress boundary condition (BC1) was maintained during cone penetration. Penetration was halted 10–20 cm above chamber bottom.

VCC test programme

The main test series (series A) examined relative densities of 75% and 90% and initial stresses ranging from 60 to 400 kPa in a full chamber. Test series D was performed using quarter chamber models with fixed cone size and particle grain size (hence fixing n_p) but variable CC diameter (variable R_d). Test series E employed half chambers to complement the main series with results at relative density of 60%. The main features of these numerical tests are collected in Table 3.

RESULTS

Raw results and post processing

The cone penetration point resistance curves recorded for test series A are collected in Fig. 4. Although the penetration resistance curves produce results that follow the expected trend (increasing resistance with confining pressure and relative density), their graphical representations are very noisy, exhibiting large oscillations.

The main source of noise in the penetration curves is particle size effect, as the analyses use a reduced n_p ratio (a few particles per cone diameter). Fig. 5 shows the result of a numerical experiment (Butlanska *et al.*, 2010) using increasingly large cones. As the ratio n_p increases, the penetration curve smooths visibly.

The oscillations are therefore a noisy artefact of the scaled discrete material and should be filtered out. A steady-state cone resistance was extracted from the raw penetration curves by fitting them with the following expression

$$q_c(h) = A(1 - e^{-Bh}) \tag{7}$$

The steady-state cone resistance is given by parameter a, collected in Table 3 for all the tests reported here. The application of this procedure is illustrated in Fig. 6.

Chamber size effect correction

Results from test series D are presented in Fig. 7. The trend of increasing limit cone resistance with R_d is similar to that observed in physical tests (e.g. Parkin & Lunne, 1982). Thus, in principle, correction for chamber size effects might be done using the same empirical correction factor CF (equation (1)) as in the physical tests. The corrected numerical cone resistance for each numerical test is then

$$q_c^*(D_R, \sigma) = \mathrm{CF}(D_R, \sigma) a(D_R, \sigma) \tag{8}$$

The correction factor had been experimentally established for a range of R_d between 33 and 120 (Jamiolkowski *et al.*, 2003). Hence its use here involves some extrapolation. To judge on the adequacy of such extrapolation the corrected cone resistance of the test in series D, q_c^*, is normalised by a reference value $q_{c\,ref}^*$, corresponding to the numerical test with highest R_d

$$q_{cn}^* = \frac{q_c^*}{q_{c\,ref}^*} \tag{9}$$

Figure 8 represents q_{cn}^* for series D as a function of R_d. If

Table 3. Characteristics and main results of the DEM-based CC-CPT tests

Series	Test identification	CC type	D_{R0}: %	p_0: kPa	D_C: m	a: MPa	CF	q_c^* (DEM): MPa	q_c^* (equation (3)): MPa
A	TEST15	1	75·2	60	1·2	6·77	2·01	13·60	16·1
A	TEST16	1	75·2	100	1·2	10·35	2·01	20·81	21·4
A	TEST17	1	76·8	200	1·2	16·14	2·05	33·12	33·1
A	TEST18	1	77·6	300	1·2	19·85	2·07	41·15	42·6
A	TEST19	1	78·4	400	1·2	22·76	2·09	47·67	51·2
A	TEST20	1	90·7	100	1·2	12·91	2·42	31·32	34·0
A	TEST21	1	91·4	140	1·2	15·33	2·44	37·48	41·9
A	TEST22	1	92·2	200	1·2	21·51	2·46	53·01	52·3
A	TEST23	1	92·9	300	1·2	25·42	2·48	63·17	67·2
D	TEST34	0·25	72·8	100	1·2	10·60	1·94	20·61	20·0
D	TEST35	0·25	86·1	100	1·2	14·80	2·30	34·07	29·7
D	TEST36	0·25	72·8	100	1·58	9·96	1·74	17·34	20·0
D	TEST38	0·25	72·0	100	0·8	8·97	2·26	20·26	19·5
D	TEST39	0·25	73·6	100	0·6	7·39	2·61	19·31	20·4
D	TEST40	0·25	72·0	100	0·4	5·73	2·97	17·04	19·5
D	TEST41	0·25	86·1	100	1·58	12·64	2·01	25·38	29·7
D	TEST43	0·25	89·9	100	0·8	11·08	2·97	32·94	33·2
D	TEST44	0·25	89·2	100	0·6	8·08	3·41	27·58	32·5
D	TEST45	0·25	86·9	100	0·4	6·38	4·04	25·77	30·4
E	TEST50	0·5	61·3	100	1·2	9·63	1·63	15·70	14·32
E	TEST51	0·5	62·4	200	1·2	15·39	1·66	25·56	21·81
E	TEST52	0·5	63·6	300	1·2	17·70	1·69	29·91	28·37
E	TEST53	0·5	64·7	400	1·2	20·55	1·72	35·36	34·43

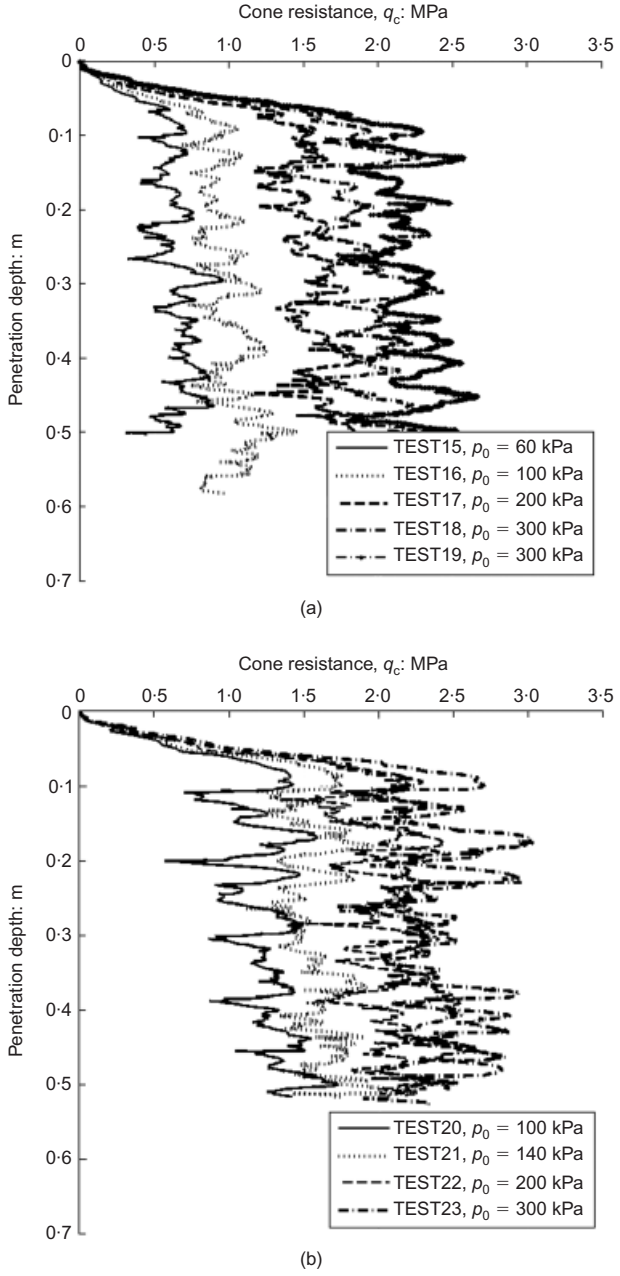

Fig. 4. Raw cone penetration resistance curves from test series A: (a) tests with target D_{R0} 75%; (b) tests with target D_{R0} 90%

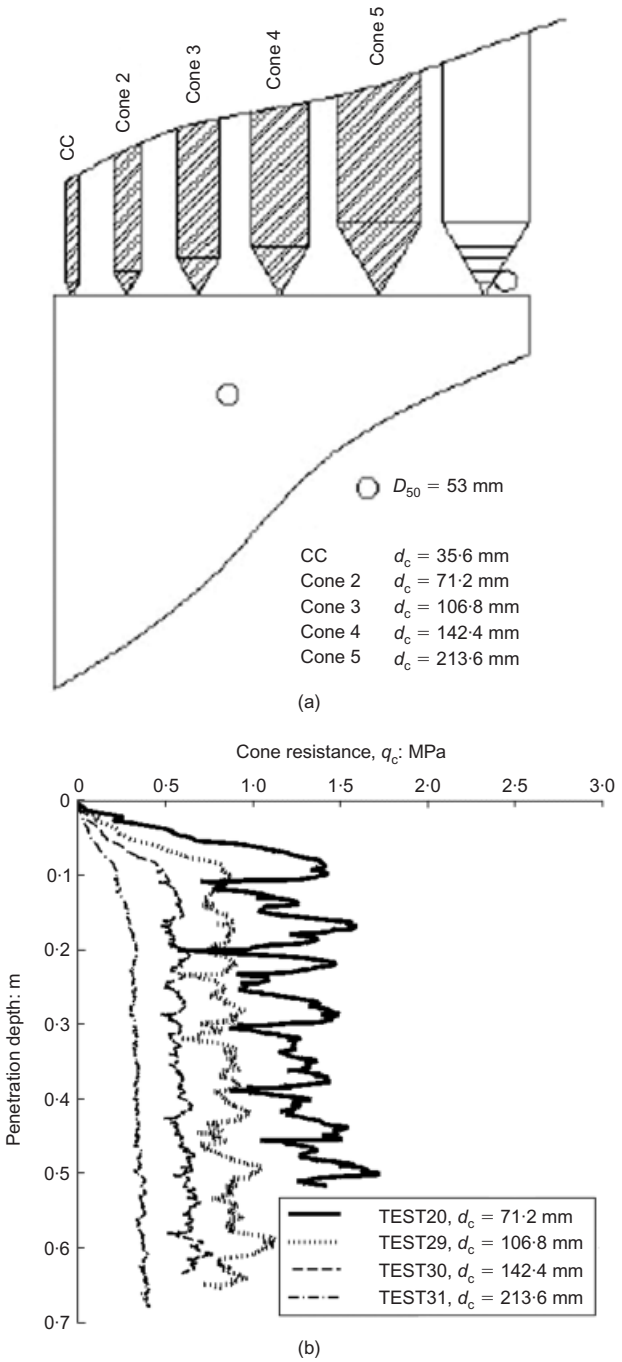

Fig. 5. Effect of increasing cone size on penetration: (a) sketch of cone sizes; (b) raw penetration curves

the CF extrapolation were perfect all values would be 1. While this is not the case, it seems that the error introduced by the extrapolation to lower R_d values of the experimental CF function is acceptable.

Comparison with physical CC results

The cone/chamber size effect correcting factors corresponding to each numerical test are collected in Table 3, alongside the resulting corrected cone resistance. Those corrected numerical steady-state cone resistance values might be now compared with the values predicted by correlation (3), based on the physical CC results. Results included in the comparison are those from the main test series A and the complementary test series E, covering a range of relative density from 60% to 90% and of confining pressure from 40 to 400 kPa. The comparison, illustrated in Fig. 9, is remarkably good, with a mean error for all tests of 7%.

CONCLUDING REMARKS

The numerical models studied here differ in several respects from the experimental CC. There was no attempt to model grain crushing. Crushing might have a secondary influence here because Ticino sand is relatively strong (ln $\sigma_c = 10{\cdot}8$, where σ_c is grain crushing strength (Jamiolkowski *et al.*, 2003)). The VCC CPT simulations have been run under isotropic confinement, after isotropic normal consolidation, whereas in the physical experiments, K_0-consolidation took place. The difference is not that important since the main stress component affecting the test result is the horizontal one (e.g. Houlsby & Hitchman, 1988). Also the K_0 condition might be more sensitive to the specific details of the implementation radial boundary condition (for instance, most physical chambers have radial stress applied through a membrane and not through a wall). Inclusion of

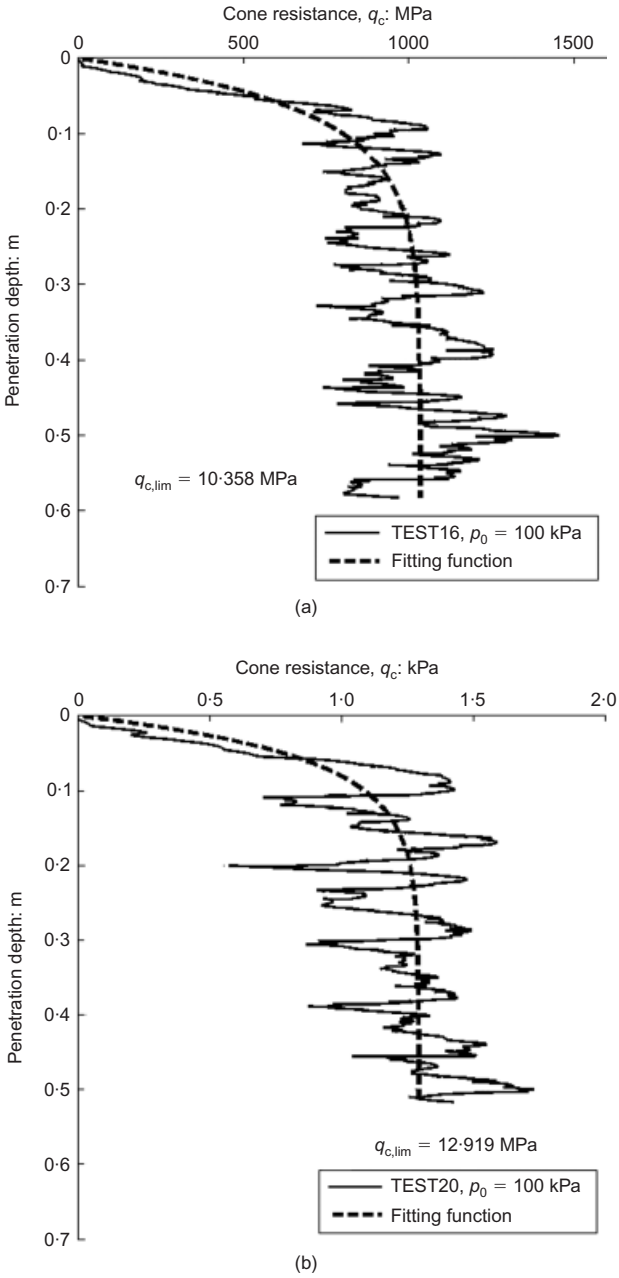

Fig. 6. Examples of curve-fit for the extraction of limit cone resistance: (a) TEST16, target D_{R0} 75%. (b) TEST20, target D_{R0} 90%

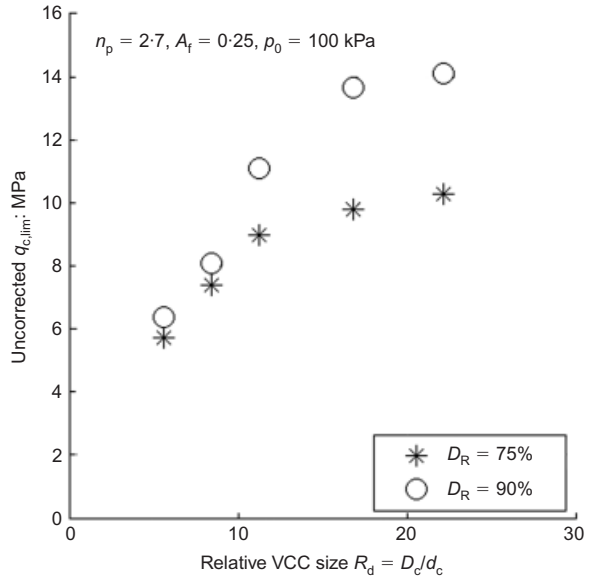

Fig. 7. Uncorrected penetration resistance obtained in test series D: quarter-cylinder simulations, fixed cone size and variable chamber size

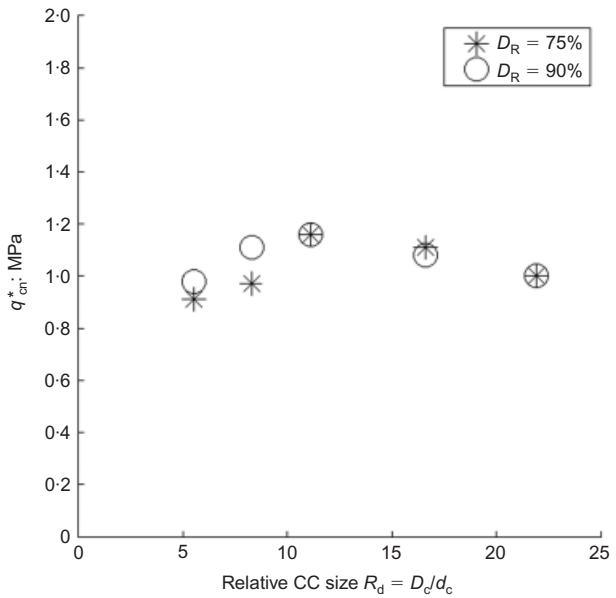

Fig. 8. Test series D, quarter-cylinder simulations. Normalised corrected cone resistance plotted against relative CC size

membrane-like boundaries in DEM models is possible (e.g. Cui *et al.*, 2007) and may be worth exploring in future VCC tests.

To the best of the present authors' knowledge these are the first reported three-dimensional CPT DEM-based simulations. The quantitative agreement obtained with physical experiments represents a remarkable improvement with respect to previous attempts, where the two-dimensional nature of the simulations made quantitative comparisons difficult. Such agreement was obtained despite the major simplifications in particle size distribution, particle behaviour and model construction required to obtain practical results using standard computers. These results seem to open a new avenue for simulation and calibration of CPT tests in granular materials. The validity of the scaling law used in this note is worthy of future exploration, particularly in relation to some aspects that have not been considered here, like shaft resistance or particle crushing.

ACKNOWLEDGEMENT

This work has been supported by the Ministry of Science and Innovation of Spain through research grant BIA2008-06537.

NOTATION

A, B	fitting parameters
a, b	functions of relative density and relative chamber size
CF	chamber size effect factor
D_c	calibration chamber diameter
D_R	relative density
d_c	cone diameter
f_G	empirical factor accounting for the grain size distribution
H	height of calibration chamber
h	penetration depth
K_{eff}	stiffness constant
k_N	normal contact stiffness
k_S	tangential contact stiffness

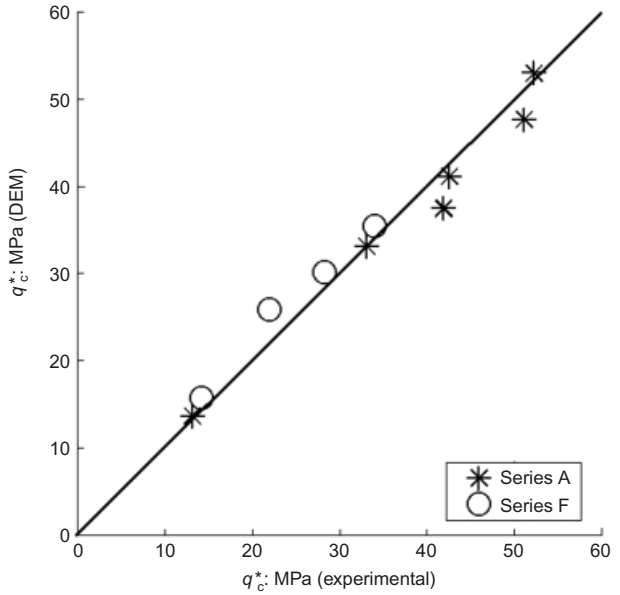

Fig. 9. Comparison between corrected cone resistance from DEM and cone resistance values predicted by correlation (3), based on the physical CC results for Ticino sand

N	number of particles
n	porosity
n_h	chamber-height-to-cone-diameter ratio
n_p	cone-diameter-to-mean-particle-diameter ratio
p_a	atmospheric pressure (100 kPa)
$q_c(h)$	steady-state cone resistance
q^*_{cn}	normalised corrected cone resistance
q^*_c	corrected cone resistance
$q^*_{c\,ref}$	reference corrected cone resistance
R_d	chamber-diameter-to-cone-diameter ratio
α	tangential-to-normal-stiffness ratio
$\Phi\mu$	interparticle friction

REFERENCES

Ahmadi, M. M., Byrne, P. M. & Campanella, R. G. (2005). Cone tip resistance in sand: modeling, verification, and applications. *Can. Geotech. J.* **42**, 977–993.

Butlanska, J. (2009). *Calibration of a discrete element model of Ticino sand*, Internal Report. Barcelona, Spain: UPC.

Butlanska, J., Arroyo, M. & Gens, A. (2009). Homogeneity and symmetry in DEM models of cone penetration. *Proc. AIP Conf. on Powders and Grains 2009* (eds M. Nakagawa and S. Luding) **1145**, 425–429.

Butlanska, J., Arroyo, M. & Gens, A. (2010). Size effects on a virtual calibration chamber. In *Numerical methods in geotechnical engineering: NUMGE 2010* (eds T. Benz & S. Nordal), pp. 225–230. Boca Raton, FL, USA: CRC Press.

Calvetti, F. (2008). Discrete modeling of granular materials and geotechnical problems. *Eur. J. Env. Civ. Engng* **12**, No. 7–8, 951–965

Calvetti, F. & Nova, R. (2005). Micro-macro relationships from DEM simulated element and in-situ tests. *Proc. 5th Int. Conf. Micromechanics of Granular Media: Powders and Grains 2005, Stuttgart* **I**, 245–250.

Cundall, P. A. (1987). Distinct element models of rock and soil structure. In *Analytical and computational methods in engineering rock mechanics* (ed. E. T. Brown), pp. 129–163. London: Allen and Unwin.

Cui, L., O'Sullivan, C. & O'Neill, S. (2007). An analysis of the triaxial apparatus using a mixed boundary three-dimensional discrete element model. *Géotechnique* **57**, No. 10, 831–844, **doi**: 10.1680/geot.2007.57.10.831.

Houlsby, G. T. & Hitchman, R. C. (1988). Calibration tests of a cone penetrometer in sand. *Géotechnique* **38**, No. 1, 39–44, **doi**: 10.1680/geot.1988.38.1.39.

Huang, A. B. & Hsu, H. H. (2004). Advanced calibration chambers for cone penetration testing in cohessionless soils. In *ISC-2 Geotechnical and geophysical site characterization* (eds A. Viana and P. W. Mayne), pp. 147–166.

Huang, A. B. & Ma, M. Y. (1994). An analytical study of cone penetration test in granular material. *Can. Geotech. J.* **31**, No. 1, 91–193.

Jamiolkowski, M., Lo Presti, D. C. F. & Manassero, M. (2003). Evaluation of relative density and shear strength of sands from CPT and DMT. In *Soil behavior and soft ground construction* (eds J. T. Germaine, T. C. Sheahan & R. V. Whitman), ASCE Geotechnical Special Publication 119, pp. 201–238. Reston, Virginia: ASCE.

Jiang, M. J., Yu, H.-S. & Harris, D. (2006). Discrete element modeling of deep penetration in granular soils. *Int. J. Numer. Anal. Meth. Geomech*. **30**, No. 4, 335–361.

Itasca (2005). *PFC3D Particle flow code in three dimensions V3·1, User's guide*. Minneapolis: Itasca Consulting Group.

Ma, M. Y. (1994). *A numerical study of cone penetration test in granular assemblies*. PhD thesis, Clarkson University, NY, USA.

Mayne, P. W. (2007). In-situ test calibrations for evaluating soil parameters. In *Characterisation and engineering properties of natural soils (3)*, pp. 1601–1652. London: Taylor & Francis.

Parkin, A. K. & Lunne, T. (1982). Boundary effects in laboratory calibration of a cone penetrometer for sand. *Proc. 2nd Eur. Symp. Penetration Testing, Amsterdam* **2**, 761–768.

Randolph, M. F. (2004). Characterisation of soft sediments for offshore applications. *Proc. 2nd Int. Conf. Site Characterisation, Porto* **1**, 209–232.

Susila, E. & Hryciw, R. D. (2003). Large displacement FEM modelling of the cone penetration test in normally consolidated sand. *Int. J. Numer. Analyt. Meth. Geomech*. **27**, No. 7, 585–602.

Ting, J. M., Corkum, B. T. & Kauffman, C. R. (1989). Discrete numerical model for soil mechanics. *J. Geotech. Engng, ASCE* **115**, No. 3, 379–398.